

Article

Efficient Carrier Recombination in InGaN Pyramidal μ -LEDs Obtained through Selective Area Growth

Jie'an Jiang^{1,2,3}, Houqiang Xu^{2,3}, Li Chen^{2,3}, Long Yan⁴, Jason Hoo⁴, Shiping Guo⁴, Yuheng Zeng^{2,3}, Wei Guo^{2,3,*}  and Jichun Ye^{2,3} 

- ¹ School of Physical Science and Technology, ShanghaiTech University, Pudong, Shanghai 201210, China; jiangjiean@nimte.ac.cn
- ² Ningbo Institute of Materials Technology and Engineering, Chinese Academy of Sciences, Ningbo 315201, China; xuhouqiang@nimte.ac.cn (H.X.); chenli@nimte.ac.cn (L.C.); yuhengzeng@nimte.ac.cn (Y.Z.); jichun.ye@nimte.ac.cn (J.Y.)
- ³ University of Chinese Academy of Sciences, Beijing 100049, China
- ⁴ Advanced Micro-Fabrication Equipment Inc., Shanghai 201201, China; longyan@amecnsh.com (L.Y.); Jasonhoo@amecnsh.com (J.H.); shipingguo@amecnsh.com (S.G.)
- * Correspondence: guowei@nimte.ac.cn

Abstract: Pyramid-shaped InGaN/GaN micro-light-emitting diodes (μ -LEDs) were grown on a sapphire substrate using the selective area growth technique. A stable emission wavelength of a single μ -LED pyramid at 412 nm was observed under an injection current from 0.05 to 20 mA, despite the non-uniformity of the thickness and composition of the multiple quantum wells (MQWs) on the sidewall. An efficient carrier confinement and, thus, a high luminescence intensity were demonstrated in the middle of the sidewall through spatial-resolved cathodoluminescence (CL) characterization and were predicted by theoretical simulations. An ultra-high output power density of 1.37 kW/cm² was obtained from the single μ -LED pyramid, illustrating its great potential for application in high-brightness micro-displays and in virtual reality and augmented reality (VR and AR) applications.

Keywords: micro-LED; selective area growth; luminescence property; output power density; carrier confinement



Citation: Jiang, J.; Xu, H.; Chen, L.; Yan, L.; Hoo, J.; Guo, S.; Zeng, Y.; Guo, W.; Ye, J. Efficient Carrier Recombination in InGaN Pyramidal μ -LEDs Obtained through Selective Area Growth. *Photonics* **2021**, *8*, 157. <https://doi.org/10.3390/photonics8050157>

Received: 17 March 2021
Accepted: 27 April 2021
Published: 10 May 2021

Publisher's Note: MDPI stays neutral with regard to jurisdictional claims in published maps and institutional affiliations.



Copyright: © 2021 by the authors. Licensee MDPI, Basel, Switzerland. This article is an open access article distributed under the terms and conditions of the Creative Commons Attribution (CC BY) license (<https://creativecommons.org/licenses/by/4.0/>).

1. Introduction

μ -LEDs have drawn an increasing amount of interest among researchers due to their wide range of applications in self-emissive micro-displays, visible light communications, virtual reality and augmented reality (VR and AR), etc. The high pixel resolution, tunability of emission wavelength, and compatibility with flexible electronics of μ -LEDs show their great advantages over conventional LEDs [1–3]. Top-down etching is one of the most commonly used techniques in fabricating μ -LEDs. For instance, Tian et al. demonstrated a GaN-based LED epitaxial structure grown on a Si substrate using a dry-etching process. In addition, 10 × 10 LED arrays with pixel diameters of 45 μ m and a peak emission at 470 nm were reported [4]. However, many previous studies indicated that the luminescence intensity and external quantum efficiency (EQE) sharply decrease with reductions in the μ -LED dimensions due to the existence of nonradiative recombination centers at the exposed sidewalls [5]. These losses originate from the point defects and dangling Ga bonds at the LED sidewalls, which are introduced during the plasma-etching process [6,7]. Wong et al. reported that plasma-enhanced chemical vapor deposition (PECVD) on the sidewall is beneficial in reducing leakage current in LEDs, but unfortunately, it has little influence on μ -LEDs with dimensions smaller than 60 × 60 μ m² [8]. Ley et al. discussed the treatment of sidewalls with KOH etching and Al₂O₃ dielectric passivation [5]. Despite the above attempts, the sidewall damages cannot be fully eliminated. A perfect alternative for avoiding the sidewall damage is the utilization of a “bottom-up” growth process.

As a typical example of a bottom-up technique, selective area growth (SAG) of μ -LEDs in the form of rods or disks offers great benefits, including an enhanced surface area for light extraction and a smooth surface morphology. Furthermore, the SAG technique can effectively reduce the threading dislocation density, which is blocked by a SiO_x or SiN_x mask [9–13]. Last of all, biaxial strain stemming from the thermal expansion and lattice mismatch during the heteroepitaxial growth can also be relieved during SAG, contributing to lower internal polarization [14–16]. Overall, SAG has been demonstrated to be a promising approach in the realization of next-generation μ -LEDs [17]. InGaN-based multiple quantum wells (MQWs) were grown on non-polar or semi-polar sidewalls of the pyramid base structure, resulting in an increased overlap of the electron and hole wavefunctions; thus, a high radiative recombination rate was obtained [18,19].

Despite the numerous advances mentioned above, there is still a lack of understanding of the correlation between the microscale optoelectronic properties of the devices and the structural information because μ -LEDs usually have stringent requirements for the uniformity of the emission wavelength. However, note that the thickness non-uniformity on the sidewalls of the SAG nanostructure is an inherent drawback for the selective area growth technique due to the variations in the gas phase and surface diffusion of In, Ga, and Al atoms [1]. Some researchers even reported multiple emission peaks and severe peak shifting during current injection [20–22]. This issue has seriously slowed down the development of μ -LEDs using the bottom-up growth technique, and a deep understanding of the spatially resolved optical and electrical behaviors of pyramid μ -LEDs is therefore, strongly, required.

In this work, electrically driven pyramidal near-UV μ -LED arrays were grown on 2 μm thick Si-doped GaN thin film on 2 inch *c*-plane sapphire with the SAG technique. A detailed analysis of the correlation between the nanoscale structural and optical properties of the pyramid μ -LEDs is provided. A strong EL intensity with a stable emission wavelength at 412 nm was reported for a single μ -LED pyramid in spite of the nonuniform thickness and composition on the semipolar crystallographic plane.

2. Materials and Methods

A pyramidal μ -LED array was grown in an AMEC Prismo HiT₃TM metal organic chemical vapor deposition (MOCVD) reactor with ambient N_2 . Trimethylaluminum, trimethylindium, trimethylgallium/triethylgallium, and ammonia were used as the precursors of Al, In, Ga, and N, respectively. A 2 μm thick Si-doped GaN thin film was grown on 2 inch *c*-plane sapphire as a current-spreading layer. A 150 nm thick SiO_2 layer serving as the mask was deposited on the top of the GaN with the e-beam evaporation technique, and the patterns were fabricated using standard photolithography followed by reactive ion etching (RIE). The diameter of the circular opening was 20 μm , and the periodicity was 40 μm . The patterned mask was then reloaded into the MOCVD reactor for regrowth. The pyramid-shaped μ -LEDs consisted of a Si-doped GaN contact layer, five periods of $\text{In}_{0.1}\text{Ga}_{0.9}\text{N}/\text{In}_{0.02}\text{Ga}_{0.98}\text{N}$ MQWs, and a p-type current-spreading layer, denoted as AlGaIn_1 and AlGaIn_2 , and they were capped with a 50 nm Mg-doped GaN contact layer. The targeted carrier concentrations for the n-GaN and p-GaN contact layers are 1×10^{19} and $2 \times 10^{18} \text{ cm}^{-3}$, respectively. The gaps between the individual μ -LEDs were filled with insulating photoresist to provide mechanical isolation. Afterwards, a thin Ni/Au (10/10 nm) p-electrode was deposited on the surface of the μ -LEDs using a shadow mask. An indium n-type electrode was coated on the exposed n-GaN template. The surface morphologies of the μ -LED pyramids were characterized by a Hitachi s4800 scanning electron microscope (SEM). The samples were optically pumped by an Ar-F (193 nm) excimer laser at various power densities. Large-scale photoluminescence (PL) spectra were collected by an optical fiber, dispersed with a Jobin-Yvon Horiba iHR550 spectrometer (300 grooves/mm), and detected by an air-cooled charge-coupled device (CCD). Spatially resolved room temperature (RT) PL analysis was carried out using a Renishaw inVia Reflex Raman microscope and spectrometer with a 325 nm He-Cd laser. In

addition, RT cathodoluminescence (CL) was analyzed with an FEI Quanta FEG 250 with a Gatan Mono CL setup. For the electrical properties, current–voltage (I–V) characterization and electroluminescence (EL) were measured with a Keithley 4200S semiconductor characterization system and a Zolix Omni-750i spectroscope, respectively. The samples for transmission electron microscopy (TEM) analysis were prepared using an FEI Helios dual-beam-focused ion-beam scanning electron microscope system with a Ga ion source. The cross-sectional morphology of the semi-polar plane, MQW layer thickness, and energy dispersion spectroscopy (EDS) mapping were characterized with an FEI probe-corrected High-Angle Annular Dark-Field (HAADF) TEM operated at an acceleration voltage of 300 kV.

3. Results

Figure 1a shows a top-view SEM image of the as-grown pyramidal μ -LED arrays. The μ -LEDs were uniformly distributed on the surface, and the facet length and pyramid height were 15 and 26 μm , respectively. The growth condition of the GaN template was similar to that of the pure GaN thin film reported in our previous work [14]. With a low V/III ratio and a low carrier gas N_2/H_2 flow ratio, the smooth semi-polar—rather than non-polar planes—were formed on the sidewall during the SAG process [17]. On the semi-polar facets, some protrusions were observed, which were possibly due to local variations in growth rates. Note that polycrystalline grains were found on top of the SiO_2 mask, which can be ascribed to the high gas-phase supersaturation and, thus, a large nucleation density [23]. A schematic illustration of the μ -LED is shown in Figure 1b.

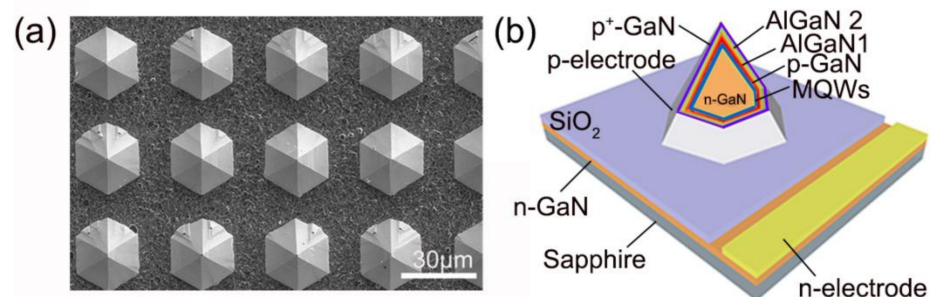


Figure 1. Top-view SEM image of the as-grown μ -LED array (a). Schematic illustration of the structure of a single μ -LED (b).

To analyze the nanoscale structural properties of the μ -LED, a cross-sectional TEM image of the pyramid is shown in Figure 2a. The zoomed-in views of the MQW regions from the upper, middle, and lower parts of the sidewall are illustrated in the HAADF images shown in Figure 2b–d, respectively, and denoted as regions A, B, and C. The regions with a brighter contrast are the high-indium quantum wells (QWs), while the regions with a darker contrast are the low-indium quantum barriers (QBs). The thicknesses of the InGaIn QW in regions A, B, and C were approximately 4, 2, and 1 nm, respectively. The corresponding GaN barriers were 7, 3, and 2 nm, respectively. The thicknesses of the MQWs decreased from region A to region C of the semi-polar plane, suggesting that gas-phase diffusion processes were more dominant over surface diffusion from the SiO_2 mask in the 3D pyramid structures, leading to thicker QWs on the top. Our result is also consistent with the observations from Wunderer et al., who established a gas-phase diffusion model during MOCVD growth [24]. It is worth noting that regions A, B, and C were just relative positions of the pyramid sidewall. The MQWs at the very bottom of the pyramid could hardly be observed because of the limited atom diffusion length. Region C was located 6 μm above the base of the μ -LED pyramid. Meanwhile, the EDS mappings of the indium content in regions A and B of the semi-polar plane are shown in Figure 2e,f. It was observed that the MQWs on the top had a stronger color contrast than in the middle. Furthermore, from the line-scan of the indium composition shown in Figure 2g, the QW

in region A had much higher indium content than in region B. The above observations suggest that a higher indium content was incorporated into the top of the pyramid. As already mentioned before, the variations in MQW thickness and composition along the semi-polar plane were induced by a limited gas diffusion towards the pyramid base, or in other words, a higher flow of precursors near the top [25,26]. This matches well with the TEM observation shown in Figure 2.

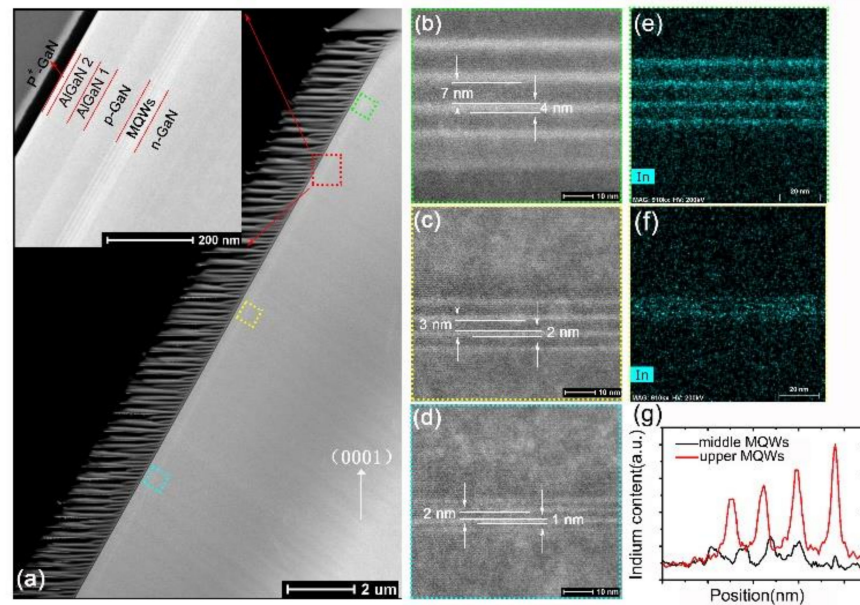


Figure 2. (a) HAADF TEM image of the semi-polar plane of a single μ -LED pyramid. The inserted image shows the low-magnification epitaxial layer containing the MQW. HAADF images of the MQW regions taken from regions A (b), B (c), and C (d) of the semi-polar planes, and corresponding EDS mappings showing the In content in regions A (e) and B (f) of the semi-polar MQWs. (g) Line scan of the In content across the MQW in the upper and middle parts of the semi-polar plane.

The optical properties of the μ -LED array were strongly correlated with the QW thickness and composition, and therefore deserve in-depth investigation. Herein, RT-PL characterization was performed. The sample was placed on an X-Y stage with a lateral resolution of 10 nm. For the power-dependent PL measurement, the 193 nm Ar-F laser illuminated at 45° towards the sample surface with an excitation area of approximately $2 \times 3 \text{ mm}^2$, covering a large number of μ -LED pyramids. The influence of the excitation power on the large-scale emission properties of the μ -LED arrays is illustrated in Figure 3a. Spontaneous emission peaks centered at 409 nm were observed, with the full width at half maximum (FWHM) value of 34 nm. Meanwhile, it is worth noting that the FWHM value of the GaN E_2 (high) Raman peak measured from the cross-sectional GaN pyramid was around 3.1 nm^{-1} , as shown in the Supplementary Information (Figure S1), which is comparable with or lower than the reports by other groups, highlighting the excellent crystal quality of the GaN pyramid [27,28]. The weak defect-related yellow luminescence (YL) at 560 nm was attributed to either carbon at the nitrogen site C_N or, simply, the isolated V_{Ga} , indicating that the defect emission is a “bulk-like” property [29,30]. As the excitation power density increased, a linear increase in PL intensity was observed, as the wavelength remained nearly constant, as shown in Figure 3b. The stable emission spectra confirmed the weak quantum-confined Stark effect (QCSE) on the semi-polar plane, as previously demonstrated [31,32]. On the other hand, an extremely weak MQW emission was observed in the planar LED sample that was directly grown on the GaN template (data not shown) under the same growth conditions. To further evaluate the nanoscale optical properties of the μ -LEDs, spatially resolved PL measurement of a single μ -LED pyramid was performed using confocal Raman spectrometry equipment. A He-Cd laser was used as the excitation

source. The wavelength and excitation power were 325 nm and 5 mW, respectively. The laser spot was focused to around 2 μm in diameter. Figure 3c shows the PL spectra obtained on different positions of the semi-polar facet. For a clear identification, the spectra in the wavelengths ranging from 400 to 480 nm are shown in the graph. The broad emission spectra could be deconvoluted into three peaks and ascribed to the emissions from the local potential minima of the non-uniform MQWs. While the laser spot moved from the top to the bottom of the semi-polar facet, both peak 1 and peak 2 of the MQW emissions followed a gradual blue shift, while the defect emission (peak 3) may have been related to the decrease in the $V_{\text{Ga-O}_N}$ complex as the position approached the bottom of the pyramid, indicating the better crystalline quality of the GaN pyramid due to the suppression of threading dislocations during the lateral epitaxial growth at the wing region [33,34]. The lateral overgrowth region during the SAG process was approximately 3 μm , as shown in Figure S2. Note that both decreasing indium content and thinning of the MQWs from top to the bottom of the semi-polar plane contributed to the blue shift of peaks 1 and 2, which corresponds perfectly with the spectral variation demonstrated in Figure 3c. The variations in the emission properties in Figure 3a,c were induced by the composition and thickness fluctuations on the sidewall of the pyramid. Efficient carrier recombination happened in the global potential minimum in the pyramid sidewall according to the macro-scale PL in Figure 3a, while the different peak positions in Figure 3c represent the radiative recombination in the local potential minimum on the pyramid [35].

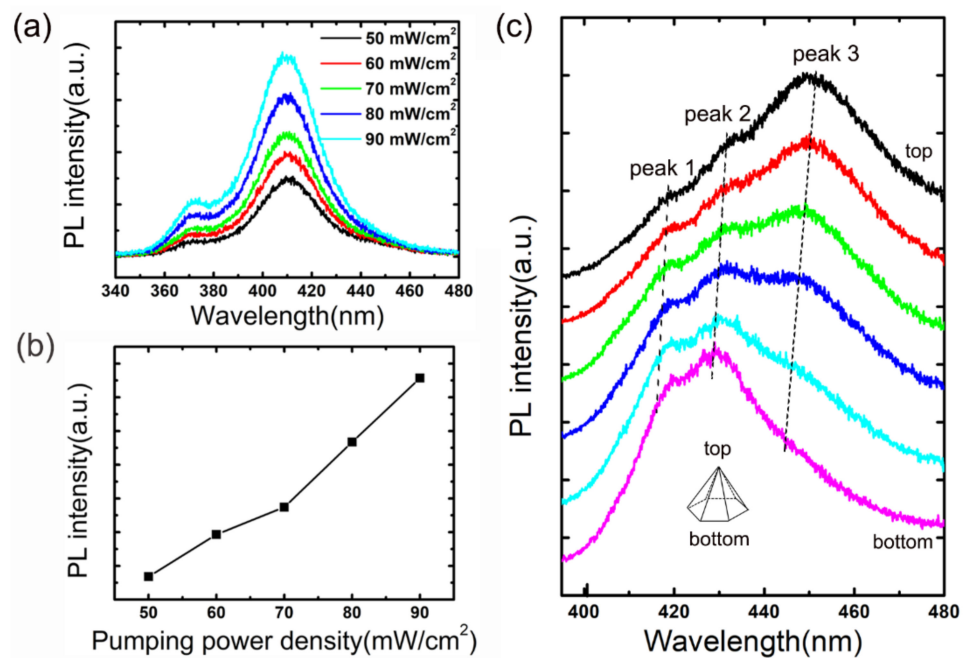


Figure 3. Macro-scale PL spectra (a), the influence of excitation power density on the PL intensity of the μ -LED array (b), and spatially resolved μ -PL spectra of a single μ -LED pyramid (c).

From the spatially resolved PL spectra shown in Figure 3c, a 12 nm peak shift was observed from the top to the bottom of the pyramid, in strong contrast to the stable 409 nm emission in the macro-scale PL spectra under various pumping powers from Figure 3a. This discrepancy is ascribed to different carrier localization effects when optical pumping was imposed on a large number of pyramids or simply on a particular position on the sidewall of the pyramid. Herein, to provide direct evidence of the relationship between the position of the facet and localized optical properties, an RT CL measurement was performed because it has a much higher lateral resolution. Figure 4a shows the top-view SEM image of a single pyramid. The position-dependent CL spectra of the semi-polar facet were performed and are shown in Figure 4b. The five dotted positions are labeled in

Figure 4a. The CL spectra revealed both the MQW emissions at 420 nm and the GaN near-band-edge emissions at 370 nm, accompanied by the weak defect-related shoulder peaks at 562 nm. When the optical pumped electron beam moved from the top to the bottom of the semi-polar facet, MQW emissions followed with a gradual blue shift, consistently with the micro-scale PL spectra shown in Figure 3c. At the very bottom of the pyramid, the MQW emissions disappeared, which is in accordance with the absence of MQWs at the bottom of the pyramid proved with TEM. Meanwhile, the FWHM of the MQW emissions of the CL spectrum on the top part was relatively broader than in the middle parts of the semi-polar facet, indicating poor carrier confinement in the top parts. Therefore, the direct correlation between the position of the MQWs and the CL spectra suggests that the carrier recombination rate is the highest in the MQWs with 1 nm QW/2 nm QB. This is ascribed to the superior carrier confinement properties in our as-grown μ -LED pyramid.

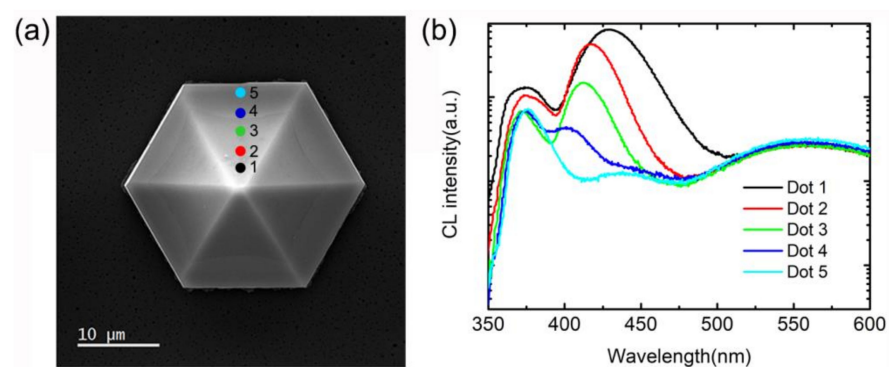


Figure 4. The top-view SEM image (a) and the position-dependent CL spectra of the semi-polar facet (b) of a single μ -LED pyramid. The five dot positions are labeled in Figure 4a.

To evaluate the electrical performance of the μ -LED, n-type and p-type Ohmic contacts were deposited on the n-GaN region and the top of the pyramid arrays, respectively. Figure 5a shows the RT EL spectra of the samples at injection currents in the range of 0.05–20 mA. The FWHM of the emission peaks decreased from 35 to 28 nm, which is much narrower than the FWHM of 43 to 53 nm from the core/shell nanowire LED fabricated with the bottom-up technique [19,36,37]. The narrow linewidth of the pyramid μ -LED greatly benefits its application in multiple-color displays, VR, and AR. A typical rectifying behavior with a turn-on voltage of 4.4 V and a series resistance of 48.5 Ω were obtained from the I-V curve of a single μ -LED, as shown in the inset image of Figure 5a. Above the turn-on voltage, a sharp increase in the forward current was observed from the I-V curve. The turn-on voltage was slightly higher than that of the planar LED. This is possibly because an indium contact was used for the convenience of testing, which had a large contact resistance and poor adherence. The light output power and peak position as a function of injection current (bottom) or current density (top) were, therefore, collected and are shown in Figure 5b. Considering the sidewall area of the pyramid, 0.05 to 20 mA current levels were transferred to current densities ranging from 3.8 A/cm² to 1.52 kA/cm². As the current increased, the peak position firstly had a blue shift from 418 to 408 nm, which can be ascribed to the band-filling effect at the beginning of the current injection; then, a slight red shift from 408 to 412 nm was observed with the increase in the current density from 0.38 to 1.52 kA/cm² due to the thermal heating effect, which caused the narrowing of the bandgap, according to the Varshni equation. Note that in previous reports, a very large peak shift of 30 nm and an 89 nm EL peak blue shift were observed in GaN μ -LEDs [38,39]. However, in this work, the EL peak shift was much smaller than expected, and the EL stability was quite good. It is well known that, unlike planar LEDs with poor overlap between the electron and hole wavefunctions, the three-dimensional geometry of the pyramid LED not only provides an efficient light extraction from the sidewall, but also suffers less from QCSE [40,41]. A single-peak EL spectrum with a negligible variation in the

peak position was demonstrated in this work. Our investigations, in fact, have provided direct evidence that, in spite of thickness and composition fluctuations, as revealed by the nanoscale PL and CL characterizations, the electrical performance of the pyramid μ -LEDs grown from the bottom up is still quite good. This can be acknowledged as a promising method for overcoming the drawbacks of plasma damage and strong QCSE in regular top-down μ -LEDs.

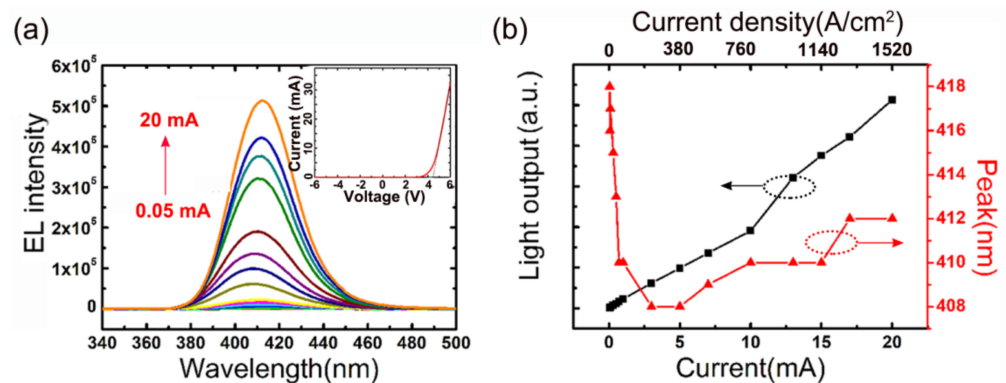


Figure 5. EL spectra of the μ -LED array with injection currents from 0.05 to 20 mA (a), where the inserted plot shows the I-V curve of the μ -LED. Light output power and peak position of a single μ -LED pyramid as a function of injection current and current density (b).

To calculate the output power of the pyramid μ -LED, the active area that emitted photons was taken into consideration. The power density of a single μ -LED pyramid could reach 1.37 kW/cm^2 under the high injection current density of 1.52 kA/cm^2 . Note that, firstly, the power density was collected from a single μ -LED pyramid with a Ni/Au (10 nm/10 nm) p-type electrode deposited on the top. Such a high output power value demonstrates the strong radiative recombination rate and a large light extraction efficiency from the 3D LED structure compared to the planar samples. Secondly, the high current density of 1.52 kA/cm^2 also suggests the stable performance of our μ -LED array. Therefore, the proposed near-UV μ -LEDs have great potential for application in high-brightness and high-efficiency micro-displays. In addition, it is worth mentioning that only a chip-on-wafer (COW) test was performed on our pyramid μ -LED in this work. The emission intensity of the single μ -LED was compared to that of a commercialized planar near-UV LED obtained by San'an optoelectronics, whose absolute output power and EQE were known. It is noted that the emitting area of the μ -LED was located on the sidewalls of the pyramid, benefiting light extraction. Thanks to the enlarged emitting area of the μ -LED, which is located on the sidewalls, and the reduced total internal reflection because of the 3D structure, higher light output power is expected. However, the EQE of our pyramid μ -LED cannot be precisely calculated due to the lack of an integrating sphere and a corresponding characterization system. Further investigations on the evaluation of the quantum efficiencies of such pyramid structures are highly desired after complete device packaging, and will be explored in the future.

Finally, to further understand the current transport and recombination mechanisms in such non-uniform MQWs, an LED structure containing a single semi-polar InGaN/InGaN QW with a thickness and indium composition gradient similar to that found in the TEM observation was simulated by numerically solving the Schrodinger and Poisson equations self-consistently [42]. The correlation between the simulated structure and the experimental morphology is shown in Figure S3. To reduce the calculation workload, the structure of our simulated LED device was simplified with a lateral dimension of $1 \mu\text{m}$ shown in the X axis and a vertical depth of $100 \mu\text{m}$ in the Z axis. The Y axis stands for the direction perpendicular to the side facet. The QW thickness decreases from 4 to 1 nm from the left to the right-hand side, following the thickness fluctuation from the top to the bottom of the sidewall facet. The schematic structure of the QW associated with the spatially resolved

distribution of the electron concentration and the radiative recombination rate inside the QW at the applied current density of 1600 A/cm^2 are illustrated in Figure 6a,b, respectively. Interestingly, the electrons are mostly concentrated near the right part of the QW, where the thickness is close to 1 nm, strongly supporting the experimental results showing that the LED luminescence is strongly localized. In the simulation process, it was assumed that the electrons are uniformly injected into the active region from the underlying n-contact layer. However, a strong variation in the radiative recombination rate is observed along the QWs with different thicknesses, suggesting a strong influence of QW thickness on carrier confinement. The EL spectra of the LED at a series of current densities are shown in Figure 6c. The peak position is around 410 nm, which is consistent with the experimental results shown in Figure 5a. Furthermore, to distinguish the contributions of the MQW composition and thickness to the optical properties of the μ -LED, structures with uniform indium compositions but increasing QW thicknesses of 1, 2, and 4 nm were designed, and the simulated EL spectra are compared in Figure 6d. The emission wavelengths are located at 408, 415, and 428 nm, respectively. Therefore, the 20 nm wavelength variation strongly supports the localized PL spectra in Figure 3c, indicating that QW thickness, rather than composition variation, plays a more important role in the luminescence properties of the μ -LED. It is noted that the wavelength of 452 nm cannot be found in both the position-dependent CL spectra shown in Figure 4b and the simulated emission spectra of the LED shown in Figure 6d. Therefore, we believe that peak 3, which is located at around 450 nm in Figure 3c, can be ascribed to emissions resulting from $V_{\text{Ga}}\text{-O}_{\text{N}}$ complex defects. Figure 6e shows the line-scan values of the electron concentration and radiative recombination rate along the QW region from left to right. The ratio between the radiative recombination rate and the electron concentration represents the relative EQE value, and this can be utilized as a gauge to optimize the QW design. The relative quantum efficiency shown by the red curve reaches the highest value at the right corner, again proving the fact that a thinner QW/QB design facilitates efficient carrier recombination. On the other hand, a thicker QW has poor control over the carrier confinement due to a low wave function overlap. This emphasizes the impact of the QW design on the luminescence properties of the μ -LED.

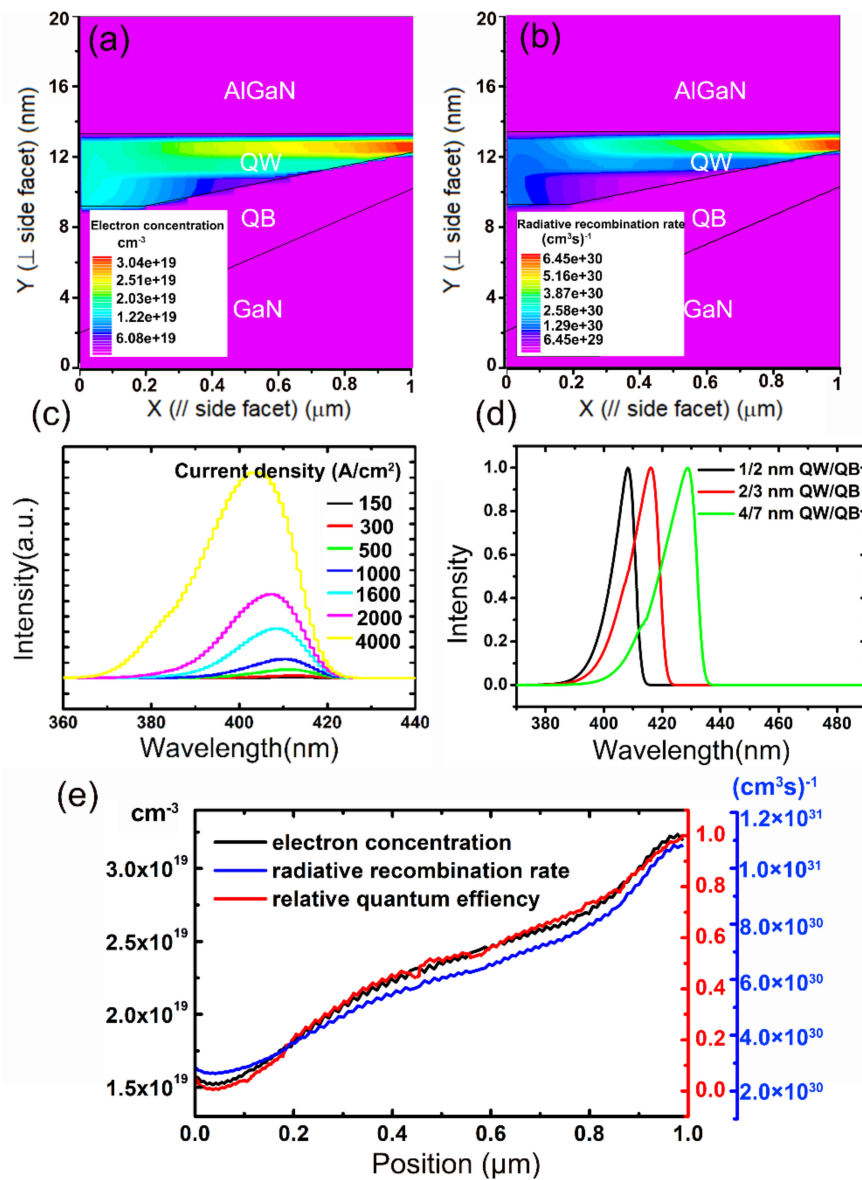


Figure 6. The schematic structure and the spatially resolved distribution of the electron concentration (a) and the radiative recombination rate (b) inside the QW region at an applied bias of 1600 A/cm². The x axis and y axis stand for the directions parallel and perpendicular to the μ-LED sidewall, respectively. Simulated emission spectra of the μ-LED at a series of injection currents (c) and normalized spectra of the LED with uniform In content and QW/QB thickness, as denoted by the labels (d). Spatially resolved electron concentration, radiative recombination rate, and relative quantum efficiency in the QW (e).

4. Conclusions

In summary, an electrically driven pyramidal InGaIn-based UV μ-LED array was grown on a sapphire substrate through a selective area growth technique. A stable emission wavelength centered at 412 nm was obtained. From spatially resolved PL spectra, the MQW emission wavelengths experienced a blue shift from the upper to the lower parts of the semi-polar plane, corresponding to the thickness and compositional fluctuations of the QWs due to the surface diffusion. The μ-LED exhibits a high output power density of 1.37 kW/cm² thanks to its large active region area and superior light extraction capability. Finally, the experimental results were further supported by a theoretical simulation, suggesting that

the carriers are efficiently confined in the thin QW regions located near the bottom of the pyramid.

Supplementary Materials: The following are available online at <https://www.mdpi.com/article/10.3390/photonics8050157/s1>, Figure S1: Raman spectrum taken from the cross-sectional GaN pyramid (a), the inserted image shows the optical image of the GaN pyramid and positions where Raman spectroscopy was taken; The Raman shift and corresponding FWHM values of the GaN E₂ (high) peak from above 10 positions on the pyramid (b); Figure S2: Cross-sectional SEM image of the pyramidal GaN overgrowing on SiO₂ mask (chemically etched away); Figure S3: The correlation between the simulation structure and the SEM cross-sectional image of the pyramid.

Author Contributions: Data curation, J.J., H.X. and L.C.; Sample growth: L.Y., J.H., S.G., Supervision, Y.Z., W.G., and J.Y.; Writing, J.J. and W.G. All authors have read and agreed to the published version of the manuscript.

Funding: This research was funded by the Youth Innovation Promotion Association CAS (2020298), Instrument Developing Project of the Chinese Academy of Sciences (YJKYYQ20190074), National Natural Science Foundation of China (61974149), Key Research and Development Program of Zhejiang Province (2020C01145), Zhejiang Provincial Natural Science Foundation of China (LQ21F040004), and Ningbo Innovation 2025 Major Project (2020Z020).

Data Availability Statement: The data that support the findings of this study are available from the corresponding author upon reasonable request.

Conflicts of Interest: The authors declare no conflict of interest.

References

1. Li, K.H.; Liu, X.; Wang, Q.; Zhao, S.; Mi, Z. Ultralow-threshold electrically injected AlGaIn nanowire ultraviolet lasers on Si operating at low temperature. *Nat. Nanotechnol.* **2015**, *10*, 140–144. [[CrossRef](#)] [[PubMed](#)]
2. Hou, Y.; Renwick, P.; Liu, B.; Bai, J. Room temperature plasmonic lasing in a continuous wave operation mode from an InGaIn/GaN single nanorod with a low threshold. *Sci. Rep.* **2014**, *4*, 5014. [[CrossRef](#)] [[PubMed](#)]
3. Koester, R.; Hwang, J.S.; Salomon, D.; Chen, X.; Bougerol, C.; Barnes, J.P.; Dang, D.; Rigutti, L.; Bugallo, A.d.; Jacopin, G.; et al. M-plane core-shell InGaIn/GaN multiple-quantum-wells on GaN wires for electroluminescent devices. *Nano Lett.* **2011**, *11*, 4839–4845. [[CrossRef](#)]
4. Tian, P.; McKendry, J.J.D.; Gong, Z.; Zhang, S.; Watson, S.; Zhu, D.; Watson, I.M.; Gu, E.; Kelly, A.E.; Humphreys, C.J.; et al. Characteristics and applications of micro-pixelated GaN-based light emitting diodes on Si substrates. *J. Appl. Phys.* **2014**, *115*, 013103. [[CrossRef](#)]
5. Ley, R.T.; Smith, J.M.; Wong, M.S.; Margalith, T.; Gordon, M.J. Revealing the importance of light extraction efficiency in InGaIn/GaN microleds via chemical treatment and dielectric passivation. *Appl. Phys. Lett.* **2020**, *116*, 251104. [[CrossRef](#)]
6. Krylyuk, S.; Paramanik, D.; King, M.; Motayed, A.; Ha, J.Y.; Bonevich, J.E.; Talin, A.; Davydov, A.V. Large-area GaN n-core/p-shell arrays fabricated using top-down etching and selective epitaxial overgrowth. *Appl. Phys. Lett.* **2012**, *101*, 071101. [[CrossRef](#)]
7. Krylyuk, S.; Debnath, R.; Yoon, H.P.; King, M.R.; Ha, J.Y.; Wen, B.; Motayed, A.; Davydov, A.V. Faceting control in core-shell GaN micropillars using selective epitaxy. *Appl. Mater.* **2014**, *2*, 071101. [[CrossRef](#)]
8. Wong, M.S.; Hwang, D.; Alhassan, A.I.; Lee, C.; Ley, R.; Nakamura, S.; DenBaars, S.P. High efficiency of III-nitride micro-light-emitting diodes by sidewall passivation using atomic layer deposition. *Opt. Express* **2018**, *26*, 21324–21331. [[CrossRef](#)] [[PubMed](#)]
9. Waag, A.; Wang, X.; Fündling, S.; Ledig, J.; Erenburg, M.; Neumann, R.; Suleiman, M.A.; Merzsch, S.; Wei, J.; Li, S.; et al. The nanorod approach: GaN Nano-LEDs for solid state lighting. *Phys. Status Solidi C* **2011**, *8*, 2296–2301. [[CrossRef](#)]
10. Jung, B.O.; Bae, S.Y.; Kato, Y.; Imura, M.; Amano, H. Morphology development of GaN nanowires using a pulsed-mode MOCVD growth technique. *CrystEngComm* **2014**, *16*, 2273–2282. [[CrossRef](#)]
11. Lin, Y.T.; Yeh, T.W.; Daniel, D.P. Mechanism of selective area growth of GaN nanorods by pulsed mode metalorganic chemical vapor deposition. *Nanotechnology* **2012**, *23*, 465601. [[CrossRef](#)]
12. Bergbauer, W.; Strassburg, M.; Kölper, C.; Linder, N.; Roder, C.; Lähnemann, J.; Trampert, A.; Fündling, S.; Li, S.F.; Wehmann, H.H.; et al. Continuous-flux MOVPE growth of position-controlled n-face GaN nanorods and embedded InGaIn quantum wells. *Nanotechnology* **2010**, *21*, 305201. [[CrossRef](#)]
13. Bae, S.Y.; Lekhal, K.; Lee, H.J.; Min, J.W.; Lee, D.S.; Honda, Y.; Amano, H. Selective-area growth of doped GaN nanorods by pulsed-mode MOCVD: Effect of Si and Mg dopants. *Phys. Status Solidi B* **2017**, *254*, 1600722. [[CrossRef](#)]
14. Jiang, J.; Xu, H.; Sheikhi, M.; Li, L.; Yang, Z.; Hoo, J.; Guo, S.; Zeng, Y.; Guo, W.; Ye, J. Omnidirectional whispering-gallery-mode lasing in GaN microdisk obtained by selective area growth on sapphire substrate. *Opt. Express* **2019**, *27*, 16195–16205. [[CrossRef](#)]

15. Bae, S.Y.; Jung, B.O.; Lekhal, K.; Kim, S.Y.; Lee, J.Y.; Lee, D.S.; Deki, M.; Honda, Y.; Amano, H. Highly elongated vertical GaN nanorod arrays on Si substrates with an AlN seed layer by pulsed-mode metal-organic vapor deposition. *CrystEngComm* **2016**, *18*, 1505–1514. [[CrossRef](#)]
16. Choi, K.; Arita, M.; Arakawa, Y. Selective-area growth of thin GaN nanowires by MOCVD. *J. Cryst. Growth* **2012**, *357*, 58–61. [[CrossRef](#)]
17. Hiramatsu, K.; Nishiyama, K.; Motogaito, A. Recent Progress in Selective Area Growth and Epitaxial Lateral Overgrowth of III-Nitrides: Effects of Reactor Pressure in MOVPE Growth. *Phys. Status Solidi A* **1999**, *176*, 535–543. [[CrossRef](#)]
18. Li, C.; Wright, J.B.; Liu, S.; Lu, P.; Figiel, J.J.; Leung, B.; Chow, W.W.; Brener, I.; Koleske, D.D.; Luk, T.; et al. Nonpolar InGaN/GaN core-shell single nanowire lasers. *Nano Lett.* **2017**, *17*, 1049–1055. [[CrossRef](#)] [[PubMed](#)]
19. Nami, M.; Stricklin, I.E.; DaVico, K.M.; Masabih, S.M.; Rishinaramangalam, A.K.; Brueck, S.R.J.; Brener, I.; Feezell, D.F. Carrier Dynamics and Electro-Optical Characterization of High-Performance GaN/InGaN Core-Shell Nanowire Light-Emitting Diodes. *Sci. Rep.* **2018**, *8*, 1–11. [[CrossRef](#)] [[PubMed](#)]
20. Li, S.F.; Fuending, S.; Wang, X.; Merzsch, S.; Al-Suleiman, M.A.M.; Wei, J.D.; Wehmann, H.H.; Waag, A.; Bergbauer, W.; Strassburg, M. Polarity and its influence on growth mechanism during MOVPE growth of GaN sub-micrometer rods. *Cryst. Growth Des.* **2011**, *11*, 1573–1577. [[CrossRef](#)]
21. Yamano, K.; Kishino, K.; Sekiguchi, H.; Oto, T.; Wakahara, A.; Kawakami, Y. Novel selective area growth (SAG) method for regularly arranged AlGaIn nanocolumns using nanotemplates. *J. Cryst. Growth* **2015**, *425*, 316–321. [[CrossRef](#)]
22. Robin, Y.; Liao, Y.; Pristovsek, M.; Amano, H. Simultaneous growth of various InGaN/GaN core-shell microstructures for color tunable device applications. *Phys. Status Solidi A* **2018**, *215*, 1800361. [[CrossRef](#)]
23. Bryan, I.; Bryan, Z.; Mita, S.; Rice, A.; Tweedie, J.; Collazo, R.; Sitar, Z. Surface kinetics in AlN growth: A universal model for the control of surface morphology in III-nitrides. *J. Cryst. Growth* **2016**, *438*, 81–89. [[CrossRef](#)]
24. Wunderer, T.; Feneberg, M.; Lipski, F.; Wang, J.; Leute, R.A.R.; Schwaiger, S.; Thonke, K.; Chuvilin, A.; Kaiser, U.; Metzner, S.; et al. Three-dimensional GaN for semipolar light emitters. *Phys. Status Solidi B* **2010**, *248*, 549–560. [[CrossRef](#)]
25. Edwards, P.R.; Martin, R.W.; Watson, I.M.; Liu, C.; Taylor, R.A.; Rice, J.H.; Na, J.H.; Robinson, J.W.; Smith, J.D. Quantum dot emission from site-controlled InGaN/GaN micropyramid arrays. *Appl. Phys. Lett.* **2014**, *85*, 4281–4283. [[CrossRef](#)]
26. Liu, W.; Mounir, C.; Rossbach, G.; Schimpke, T.; Avramescu, A.; Lugauer, H.-J.; Strassburg, M.; Schwarz, U.; Deveaud, B.; Jacopin, G. Spatially dependent carrier dynamics in single InGaN/GaN core-shell microrod by time-resolved cathodoluminescence. *Appl. Phys. Lett.* **2018**, *112*, 052106. [[CrossRef](#)]
27. Hoffmann, A.; Siegle, H.; Kaschner, A.; Eckey, L.; Sawaki, N. Local strain distribution of hexagonal GaN pyramids. *J. Cryst. Growth* **1998**, *189*, 630–633. [[CrossRef](#)]
28. Tian, P.; Edwards, P.R.; Wallace, M.J.; Martin, R.W.; Mckendry, J.; Gu, E. Characteristics of GaN-based light emitting diodes with different thicknesses of buffer layer grown by HVPE and MOCVD. *J. Phys. D Appl. Phys.* **2017**, *50*, 075101. [[CrossRef](#)]
29. Reddy, P.; Hoffmann, M.P.; Kaess, F.; Bryan, Z.; Bryan, I.; Bobea, M.; Klump, A.; Tweedie, J.; Kirste, R.; Mita, S.; et al. Point defect reduction in wide bandgap semiconductors by defect quasi Fermi level control. *J. Appl. Phys.* **2016**, *120*, 185704. [[CrossRef](#)]
30. Li, Q.; Wang, G.T. Spatial distribution of defect luminescence in GaN nanowires. *Nano Lett.* **2010**, *10*, 1554–1558. [[CrossRef](#)] [[PubMed](#)]
31. Zhu, S.; Lin, S.; Li, J.; Yu, Z.; Cao, H.; Yang, C.; Li, J.; Zhao, L. Influence of quantum confined Stark effect and carrier localization effect on modulation bandwidth for GaN-based LEDs. *Appl. Phys. Lett.* **2017**, *111*, 171105. [[CrossRef](#)]
32. Tangi, M.; Mishra, P.; Janjua, B.; Prabaswara, A.; Zhao, C.; Priante, D.; Min, J.; Ng, T.K.; Ooi, B.S. Role of quantum-confined stark effect on bias dependent photoluminescence of N-polar GaN/InGaN multi-quantum disk amber light emitting diodes. *J. Appl. Phys.* **2018**, *123*, 105702. [[CrossRef](#)]
33. Baek, H.; Lee, C.-H.; Chung, K.; Yi, G.-C. Epitaxial GaN Microdisk Lasers Grown on Graphene Microdots. *Nano Lett.* **2013**, *13*, 2782–2785. [[CrossRef](#)] [[PubMed](#)]
34. Reshchikov, M.A.; Morkoc, H. Luminescence properties of defects in GaN. *J. Appl. Phys.* **2005**, *97*, 061301. [[CrossRef](#)]
35. Debusmann, R.; Brauch, U.; Hoffmann, V.; Weyers, M.; Kneissl, M. Spacer and well pumping of InGaIn vertical cavity semiconductor lasers with varying number of quantum wells. *J. Appl. Phys.* **2012**, *112*, 033110. [[CrossRef](#)]
36. Chen, W.; Hu, G.; Jiang, J.; Liu, M.; Yang, Y. Electrically Driven Single Pyramid InGaIn/GaN Micro Light-Emitting Diode Grown on Silicon Substrate. *J. Disp. Technol.* **2015**, *11*, 285–291. [[CrossRef](#)]
37. Chen, W.; Lin, J.; Chen, Y.; Han, X.; Zhang, B. Dual-color InGaIn/GaN pyramidal micro light-emitting diode selectively grown on SiO₂ masked Si substrate. *J. Disp. Technol.* **2015**, *12*, 1. [[CrossRef](#)]
38. Chung, K.; Yoo, H.; Hyun, J.K.; Oh, H.; Tchoe, Y.; Lee, K.; Baek, H.; Kim, M.; Yi, G.-C. Flexible GaN Light-Emitting Diodes Using GaN Microdisks Epitaxially Laterally Overgrown on Graphene Dots. *Adv. Mater.* **2016**, *28*, 7688–7694. [[CrossRef](#)]
39. Bae, S.; Kim, D.; Lee, D.; Lee, S.; Baek, J.H. Highly Integrated InGaIn/GaN Semipolar Micro-Pyramid Light-Emitting Diode Arrays by Confined Selective Area Growth. *Electrochem. Solid-State Lett.* **2012**, *15*, H47–H50. [[CrossRef](#)]
40. Waltereit, P.; Brandt, O.; Trampert, A.; Grahn, H.T.; Ploog, K.H. Nitride semiconductors free of electrostatic fields for efficient white light-emitting diodes. *Nature* **2000**, *406*, 865–868. [[CrossRef](#)] [[PubMed](#)]
41. Speck, J.S.; Chichibu, S.F. Nonpolar and Semipolar Group III Nitride-Based Materials. *MRS Bull.* **2009**, *34*, 304–309. [[CrossRef](#)]
42. Guo, W.; Mitra, S.; Jiang, J.; Xu, H.; Sheikhi, M.; Sun, H.; Tian, K.; Zhang, Z.; Jiang, H.; Roqan, I.; et al. Three-dimensional band diagram in lateral polarity junction III-nitride heterostructures. *Optica* **2019**, *6*, 1058. [[CrossRef](#)]